

Near-circularly-polarized attosecond pulse generation from carbon monoxide molecules with a combination of linearly and circularly polarized fields

Ning Sun,¹ Xiaosong Zhu,^{1,*} Bincheng Wang,¹ Dian Wang,¹ Renzhi Shao,¹ Pengfei Lan,^{1,†} and Peixiang Lu^{1,2}

¹Wuhan National Laboratory for Optoelectronics and School of Physics, Huazhong University of Science and Technology, Wuhan 430074, China

²Hubei Key Laboratory of Optical Information and Pattern Recognition, Wuhan Institute of Technology, Wuhan 430205, China



(Received 6 November 2019; accepted 11 May 2020; published 28 May 2020)

We investigate the polarization properties of high harmonics generated from oriented carbon monoxide molecules driven by a linearly polarized laser field combined with a weaker circularly polarized high-frequency assistant laser field (LPCP). The results show that the harmonics with higher ellipticities are obtained close to the cutoff region. Further analysis shows that the results are due to the manipulation of the electron trajectory by the LPCP field and the molecular asymmetric structure. By taking advantage of the properties above, we propose and theoretically demonstrate a method to generate attosecond extreme ultraviolet pulses with large ellipticity. Because of the difference of harmonic ellipticities contributed from the long and short trajectories, an even higher harmonic ellipticity can be obtained by filtering the long trajectory. In addition, by adjusting the relative phase between linearly polarized and circularly polarized fields, the attosecond XUV pulse varies from being left-elliptically polarized to right-elliptically polarized.

DOI: [10.1103/PhysRevA.101.053437](https://doi.org/10.1103/PhysRevA.101.053437)

I. INTRODUCTION

High-order harmonic generation (HHG) is a highly nonlinear process that up-converts intense the infrared laser field into the extreme ultraviolet (XUV) and soft x-ray radiation [1–3]. The generated harmonic spectrum containing abundant information about the structure and dynamics of the target has been widely employed for the ultrafast detection in atoms [4–6], in molecules [7–11], and in solids [12–14]. In recent decades, HHG from atoms and molecules has been intensively studied for its potential applications in generating coherent attosecond pulses (APs) [15–17]. The availability of APs has provided an unprecedented temporal resolution for probing ultrafast processes of physics and chemistry. For instance, by using the newly developed tools of attosecond metrology, one can experimentally observe the electron tunneling in atoms with sub-femtosecond temporal resolution [18].

To date, nearly-circularly-polarized HHG and APs have numerous important applications, e.g., chiral recognition [19,20] and differential measurements of circular dichroism of molecules [21,22]. Therefore, the study of the generation of nonlinearly polarized APs has attracted general interest in recent years. Due to the rescattering mechanism of the HHG process, the efficiency of HHG is decreased compared to that applying an LP laser field [23,24]. Some methods have been proposed to overcome this problem. Nearly-circularly-polarized AP [25] and elliptically polarized AP with ultrafast helicity oscillation [26] have been theoretically demonstrated by taking advantage of ring-current states. Circularly polarized (CP) high-order harmonics can also be generated by combining an elliptically polarized laser field with strong

static fields or a few-cycle elliptically polarized laser field with terahertz fields from molecular media [27]. Resonant below-threshold HHG in elliptical laser fields also holds great potential for creating CP XUV sources [19]. Apart from these works, it has been demonstrated that CP APs can be generated with a bichromatic counterrotating circularly polarized (BCCP) driving laser field [22,28–31]. However, the two adjacent harmonics gain opposite helicities in this scheme, which will decrease the ellipticity of the synthesized AP. In recent works, HHG driven by two noncollinear beams with counterrotating circular polarization can directly generate CP harmonics with opposite helicities separated in space [21,32,33].

In this paper, we propose and investigate a scheme for the generation of highly elliptically polarized APs. Specifically, we use a combined laser field composed of a strong LP component with a weaker CP assistant component (LPCP field) interacting with oriented CO molecules to generate CP high-order harmonics close to the cutoff region. From this, one can efficiently generate both a highly elliptically polarized attosecond pulse train (APT) by using a long LPCP field and a highly elliptically isolated polarized attosecond pulses (IAPs) by using around 10-fs LPCP driving field. Because of the difference of harmonic ellipticities contributed to by the long and short trajectories, an even higher harmonic ellipticity can be obtained by filtering the long trajectory. In addition, by adjusting the relative phase between linearly polarized and circularly polarized fields, the ellipticity of the attosecond XUV pulse can be tuned in a wide range.

II. THEORETICAL MODEL

In our simulations, we investigate HHG based on the two-dimensional time-dependent Schrödinger equation (TDSE)

*zhuxiaosong@hust.edu.cn

†pengfeilan@hust.edu.cn

[34]

$$i \frac{\partial \Psi(\mathbf{r}, t)}{\partial t} = H(\mathbf{r}, t) \Psi(\mathbf{r}, t). \quad (1)$$

Atomic units (a.u.) are used throughout this paper. $H(\mathbf{r}, t)$ is the length gauge time-dependent Hamiltonian given by

$$H(\mathbf{r}, t) = -\frac{1}{2} \nabla^2 + V(\mathbf{r}) - \mathbf{r} \cdot \mathbf{E}(t). \quad (2)$$

The highest occupied molecular orbital (HOMO) of target molecule CO is modeled by a soft-core potential [35], which has the form in the Cartesian coordinates

$$V(\mathbf{r}) = -\frac{(Z_{1i} - Z_{1o})e^{-[(\mathbf{r}-\mathbf{R}_1)^2/\rho]} + Z_{1o}}{\sqrt{\xi + (\mathbf{r} - \mathbf{R}_1)^2}} - \frac{(Z_{2i} - Z_{2o})e^{-[(\mathbf{r}-\mathbf{R}_2)^2/\rho]} + Z_{2o}}{\sqrt{\xi + (\mathbf{r} - \mathbf{R}_2)^2}}. \quad (3)$$

Here $Z_{1i} = 6$, $Z_{1o} = 0.6$ and $Z_{2i} = 4$, $Z_{2o} = 0.4$ denote the bare charge and the effective nuclear charge as seen by an electron at infinite distance for the O center and the C center, respectively. The subscripts i and o denote the inner and outer limits of Z_1 and Z_2 . \mathbf{R}_1 and \mathbf{R}_2 are the positions of the nuclei. $\xi = 0.5$ and $\rho = 1/1.746$ are the softening and the screening parameters. $\mathbf{r} \equiv (x, y)$ denotes the electron position in the two-dimensional x - y plane.

We use the split-operator method to solve the TDSE [34]. We obtain the ground state by imaginary time propagation. The calculated ionization potential is 14.5 eV, agreeing well with the experimental value of CO. The LPCP laser field vector polarized in the x - y plane is defined by $\mathbf{E}(t) = f(t)\{[E_1 \cos(\omega t + \Delta\phi) + E_2 \cos(2\omega t)]\hat{\mathbf{x}} - E_2 \sin(2\omega t)\hat{\mathbf{y}}\}$, where E_1 is the amplitude of the LP laser field, E_2 is the amplitude of the CP laser field, and ω is the frequency of the LP pulse. The CP pulse with the frequency 2ω rotates clockwise. $f(t)$ is the envelope of the pulse. $\Delta\phi$ is the relative phase between LP and CP fields.

To avoid spurious reflections from the spatial boundaries, the electron wave function $\Psi(\mathbf{r}, t)$ is multiplied by a mask function G with the following form [36]:

$$G = g_x(x)g_y(y) \quad (4)$$

at each time step, in which

$$g_x(x) = \begin{cases} 1 & |x| < R_x - L_x \\ \sin^{1/8} \left(\frac{\pi(R_x - |x|)}{2L_x} \right) & |x| \geq R_x - L_x \end{cases} \quad (5)$$

and

$$g_y(y) = \begin{cases} 1 & |y| < R_y - L_y \\ \sin^{1/8} \left(\frac{\pi(R_y - |y|)}{2L_y} \right) & |y| \geq R_y - L_y \end{cases}. \quad (6)$$

For all results reported here, we set the width of the ‘‘absorbing’’ area as $L_x = 45$ a.u. and $L_y = 45$ a.u. The range of the ‘‘mask function’’ is from -135 a.u. to 135 a.u., i.e., $R_x = R_y = 135$ a.u.. The space step is $dx = dy = 0.13$ a.u. and the time step is $dt = 0.05$ a.u. in our simulations. The time-dependent dipole acceleration can be obtained by means of the Ehrenfest theorem

$$A_q(t) = -\langle \Psi(t) \| H(t), [H(t), q] \| \Psi(t) \rangle, \quad q = x, y. \quad (7)$$

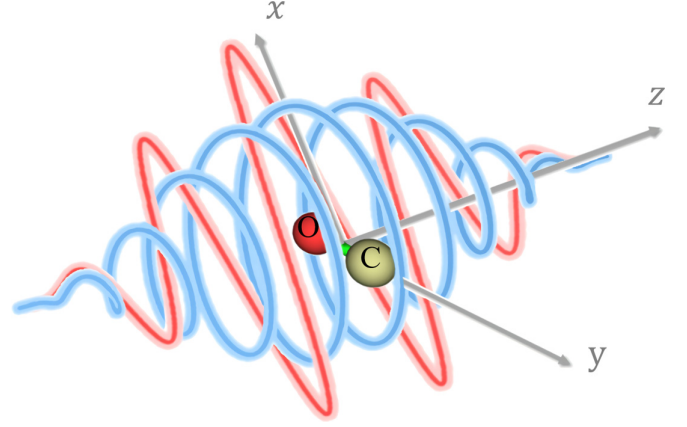


FIG. 1. Schematic diagram of a CO molecule in the LPCP field. The molecule is oriented along the y axis. The incident fundamental frequency laser is linearly polarized along the x axis, the other weaker laser field circularly is polarized in the x - y plane and their propagation directions are along the z axis.

Then, the HHG is obtained by Fourier-transforming the dipole acceleration

$$a_q(\omega_n) = \int A_q(t) \exp(-i\omega_n t) dt, \quad (8)$$

with $\omega_n = \frac{2n\pi}{T_0}$, $n = 1, 2, \dots$, and T_0 is the optical cycle of the fundamental laser field. The intensity of left- and right-circularly-polarized harmonic components can be obtained by

$$I_{\pm} = |a_{\pm}|^2, \quad (9)$$

where $a_{\pm} = \frac{1}{\sqrt{2}}(a_x \pm ia_y)$. The ellipticity of high-order harmonics can be obtained as [37,38]

$$\epsilon = \frac{|a_+| - |a_-|}{|a_+| + |a_-|}. \quad (10)$$

The rotation direction of the electric field can be quantitatively described by the helicity, which is defined as

$$h = \text{sgn}(\epsilon). \quad (11)$$

The helicity h takes the values -1 and 1 , indicating the two opposite rotation directions.

III. RESULTS AND DISCUSSIONS

A. Properties in the spectral domain

A sketch of the systems is presented in Fig. 1. The CO molecule is oriented along the y axis. The incident fundamental frequency laser is linearly polarized along the x axis, the other weaker laser field is circularly polarized in the x - y plane and their propagation directions are along the z axis.

The HHG driven by the LPCP laser field is shown in Fig. 2. The fundamental laser wavelength is $\lambda_1 = 800$ nm and laser intensity is $I_1 = 2.5 \times 10^{14}$ W/cm². The assistant laser wavelength is $\lambda_2 = 400$ nm and laser intensity is $I_2 = 1.75 \times 10^{14}$ W/cm². The relative phase $\Delta\phi$ is 0.2π . The envelope is trapezoidal with a two-cycle rising and a two-cycle falling edge and a three-cycle plateau (in units of the optical cycle

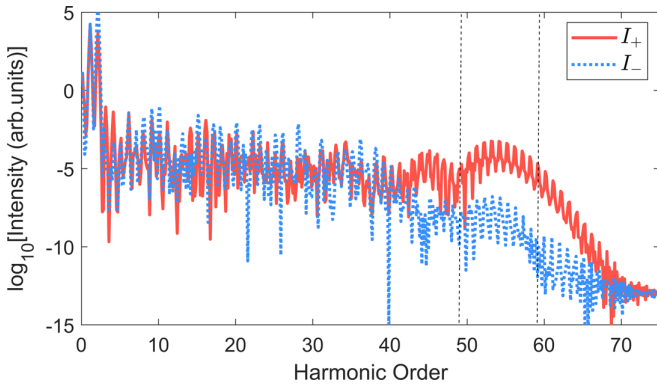


FIG. 2. The spectra of the left-circularly-polarized harmonics (blue dashed line) and the right-circularly-polarized harmonics (red solid line) from CO molecules in the LPCP field.

of fundamental laser field). The left- and right-circularly-polarized harmonics are presented by blue dashed and red solid lines, respectively. One can see that the intensity of the right-circularly-polarized component is much larger than that of the left-circularly-polarized component ranging from the 49th-order (presented by the dashed line) to the 59th-order (presented by the dashed line). The harmonic ellipticity is as high as 0.90 close to the cutoff region.

To analyze the reason why the ellipticity of the harmonics close to the cutoff region is very high, we present the time-frequency distribution of the HHG in Fig. 3(a) with the Gabor transform. The color map of Fig. 3(a) represents the time-frequency distribution in the logarithmic scale. Considering the dipole acceleration $A_q(t)$ of Eq. (7), the Gabor transform is performed as [39]

$$GT_q[\Omega, t_0] = \frac{1}{2\pi} \int dt A_q(t) e^{-i\Omega t} e^{-(t-t_0)^2/2\sigma^2}, \quad (12)$$

where Ω is the frequency of the high-order harmonics. In our study, we use $\sigma = 1/4\omega$. The time-frequency distribution is obtained by

$$\begin{aligned} I_{GT}[\Omega, t_0] &= I_{GT_x}[\Omega, t_0] + I_{GT_y}[\Omega, t_0] \\ &= \sum_{q=x,y} |GT_q[\Omega, t_0]|^2. \end{aligned} \quad (13)$$

The ellipticity distribution is obtained by $\epsilon = \frac{|GT_+| - |GT_-|}{|GT_+| + |GT_-|}$, in which $GT_{\pm} = 1/\sqrt{2}(GT_x \pm iGT_y)$. The time-frequency distribution shows that the cutoff energy of the harmonic radiation in one-third of the optical cycle is much higher than those in the latter two-thirds of the optical cycle due to the asymmetry of the LPCP field. To explain the manipulation of the electron trajectory by the LPCP laser field, we calculate the classical recombination paths by solving Newton's equation [40] under the LPCP laser field in Fig. 3(b). The classical recombination times of the electrons are presented by the red hollow circles. One can see three recombination bursts appear in one optical cycle and the burst in one-third of the optical cycle has the highest recombination energy, which coincides with the results of Fig. 3(a). To discuss the time-frequency properties of the harmonic ellipticity close to the cutoff region, we present time-frequency distribution of the harmonic ellipticity

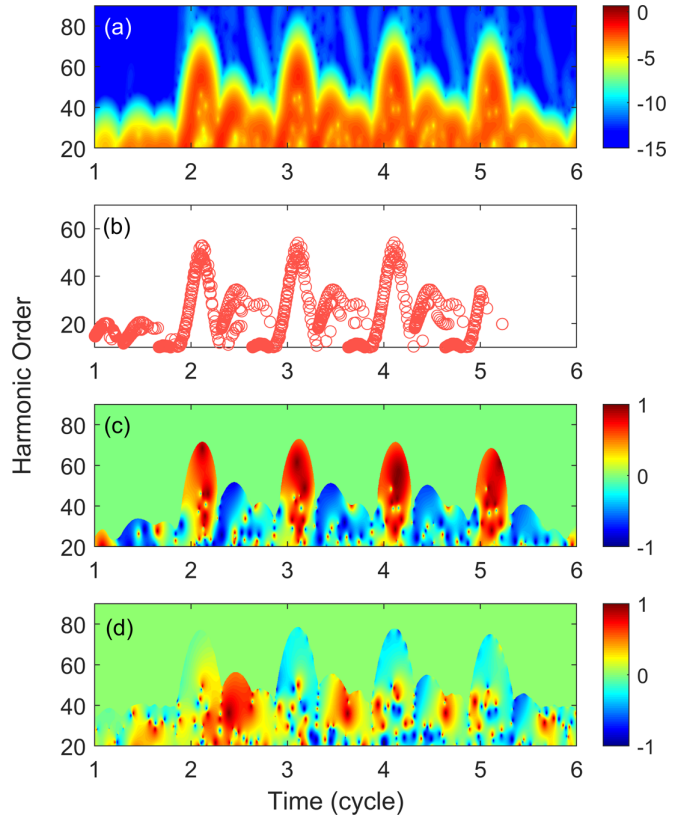


FIG. 3. Analysis of HHG from CO molecule and Kr atom. (a) The time-frequency distribution of the HHG. (b) The classical behaviors of the electrons by solving Newton's equation under the LPCP laser field. (c) The time-frequency distribution of the harmonic ellipticity from CO molecule. (d) The time-frequency distribution of the harmonic ellipticity from the Kr atom.

in Fig. 3(c). The bursts with the highest cutoff energy not only exhibit the same helicity but also exhibit very high ellipticity. Therefore, we demonstrate that the generation of high-order harmonics with higher ellipticities benefits from manipulation of the classical electron trajectory in the LPCP field. In contrast, if an LP laser field is used, two bursts per cycle have the same cutoff energy and opposite helicities despite they both have high ellipticities. In addition, it is found that the intensities for the long and short trajectories are comparable, but the ellipticity for the long trajectory is higher than that for the short trajectory. Further analysis on the HHG contributed from short and long trajectories is discussed in Sec. III B.

To further reveal the contribution of the symmetries of the molecular orbitals to high ellipticity, we compare the HHG from CO and the reference atom Kr because the two targets have similar ionization energies and different orbital symmetries. We first compare the results based on TDSE [34]. The Kr atom is also modeled by a soft-core potential [41,42] with a soft-core parameter of 4.15 to obtain the ionization potential of Kr $I_p = 0.5145$ a.u. Since, in a neutral atom, all the degenerate p orbitals are occupied, both the $4p_x$ and $4p_y$ states contribute to the HHG. We present the time-frequency distribution of the harmonic ellipticity from Kr in Fig. 3(d). It is shown that the bursts from Kr have the same structure as that from CO but the harmonic ellipticities in Fig. 3(d) are

close to 0. This further indicates that the ellipticity is related to the symmetry of the orbitals.

The TDSE calculation is two-dimensional, which reflects the symmetry effect of the orbitals of CO and Kr atom. However, the orbitals in this model still have difference from the real orbitals. To describe the effect of symmetry with more accurate orbitals, the real orbitals for CO and Kr, obtained by an *ab initio* calculation using a 6-31G* basis set in the GAUSSIAN software package [43], are chosen as the ground states in the calculation below. From this, we calculate the induced dipole moments D_q^\pm contributing to the right- and left-circularly-polarized components of different harmonic orders [44,45].

$$D_q^\pm = P(\mathbf{k}_s, t_s, t'_s) \times d_{\text{ion}}[\mathbf{v}(\mathbf{k}_s, t'_s)] e^{-iS(\mathbf{k}_s, t'_s, t_s)} d_{\text{rec}}^\pm[\mathbf{v}(\mathbf{k}_s, t_s)], \quad (14)$$

with the complex-valued times of ionization t'_s , recombination t_s , and momentum $\mathbf{k}_s = -\int_{t'_s}^{t_s} dt'' \mathbf{A}(t'') / (t_s - t'_s)$. The velocity of the electron is $\mathbf{v}(\mathbf{k}, t) = \mathbf{k} + \mathbf{A}(t)$ with $\mathbf{A}(t) = -\int^t \mathbf{E}(t') dt'$. The times of ionization t'_s and recombination t_s are given as solutions of the corresponding saddle-point equations [46,47]

$$\mathbf{v}(\mathbf{k}_s, t'_s)^2 / 2 = -I_p, \quad (15)$$

$$\mathbf{v}(\mathbf{k}_s, t_s)^2 / 2 = q\omega - I_p, \quad (16)$$

with the harmonic order q and the ionization potential I_p . Specifically, we choose the long or short trajectory by selecting the saddle times of ionization t'_s and recombination t_s . In Eq. (14), the term $d_{\text{ion}}[\mathbf{v}(\mathbf{k}_s, t'_s)]$ is defined by $d_{\text{ion}} = \langle \mathbf{v}(\mathbf{k}_s, t'_s) | \Psi_0 \rangle$. Ψ_0 is the ground state of the target molecule CO or the atom Kr. In the third term e^{-iS} of Eq. (14), S is defined by $S(\mathbf{k}_s, t'_s, t_s) = \int_{t'_s}^{t_s} dt' [\mathbf{v}(\mathbf{k}_s, t_s) - \mathbf{A}(t')]^2 / 2 + I_p$. The last term is $d_{\text{rec}}^\pm = \langle \Psi_0 | \mathbf{e}_\pm^* \cdot \mathbf{d} | e^{i\mathbf{v}(\mathbf{k}_s, t_s) \cdot \mathbf{r}} \rangle$, where the dipole operator \mathbf{d} is projected on the relevant polarization vector $\mathbf{e}_\pm = \frac{1}{\sqrt{2}}(\mathbf{e}_x \pm i\mathbf{e}_y)$. In addition to these, the prefactor $P(\mathbf{k}_s, t_s, t'_s)$ includes all other factors that are independent of the molecular or atomic orbitals. To reveal the role of the ground state on the harmonic ellipticity, we only need to consider two terms of the induced dipole moments which are dependent on the molecular or atomic orbital. These two terms are defined by $\mathcal{D}_q^\pm = d_{\text{ion}} \cdot d_{\text{rec}}^\pm$. Since the amplitudes of the $|\mathcal{D}_q^\pm|^2$ approximately reflect the intensities of the left- and right-circularly-polarized components for harmonics, we simply calculate the ratio defined by $ratio = |\mathcal{D}_q^+|^2 / |\mathcal{D}_q^-|^2$. We present the ratios for the long and short trajectories from CO and Kr in Figs. 4(a) and 4(b). One can see the much smaller ratios in the case of Kr, as compared to CO. Resulting from the isotropic structure of Kr 4*p* states, the ratios are close to 1, i.e., the amplitudes of the $|\mathcal{D}_q^\pm|^2$ of Kr are comparable. But for CO, due to its asymmetric orbital structure, one can see that the ratios are much larger than 1, i.e., $|\mathcal{D}_q^\pm|^2$ are significantly different, and the bursts in Fig. 3(c) gain high ellipticities [38,48]. This is because the phase difference between the two orthogonal HHG components is close to 0 or π from a symmetric orbital, while the phase difference can be close to $\pi/2$ from an asymmetric orbital as in the details discussed in Ref. [48]. In addition, it is found that the ratios for

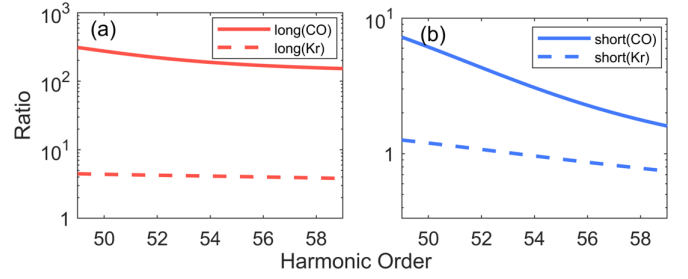


FIG. 4. Comparison of the ratios from CO molecule and Kr atom. (a) The ratios of $|\mathcal{D}_q^+|^2$ for the long trajectory contributed from target molecule CO and atom Kr. (b) The ratios of $|\mathcal{D}_q^+|^2$ for the short trajectory from target molecule CO and atom Kr.

the long trajectory are larger than those for the short trajectory. This issue will be studied further in the next section.

In addition, we compared the HHG with that in the BCCP field with the same laser intensities and wavelengths in Fig. 5. The BCCP laser field vector polarized in the x - y plane is defined by $\mathbf{E}(t) = f(t)\{[E_1 \cos(\omega t + \Delta\phi) + E_2 \cos(2\omega t)]\hat{\mathbf{x}} + [E_1 \sin(\omega t) - E_2 \sin(2\omega t)]\hat{\mathbf{y}}\}$. The intensity of the fundamental component is $I_1 = 2.5 \times 10^{14}$ W/cm² and the intensity of the assistant component is $I_2 = 1.75 \times 10^{14}$ W/cm². The relative phase $\Delta\phi$ is 0.2π . The envelope $f(t)$ is trapezoidal with a two-cycle rising and a two-cycle falling edge and a three-cycle plateau (in units of the optical cycle of fundamental laser field). It is found that the HHG with the LPCP scheme not only has the comparable intensity in the plateau region as that with the BCCP scheme, which has been widely applied in experiments for HHG, but also has a much wider spectrum range. This implies that the HHG in the LPCP field is favorable to generate APs.

B. Attosecond pulses

By taking advantage of the properties above, a highly elliptically polarized APT can be obtained by filtering the harmonics from the 49th order to the 59th order. The three-dimensional (3D) plot of the electric field of the generated APT is presented in Fig. 6. The full width at half maximum (FWHM) of each pulse in the train is around 280 as. The

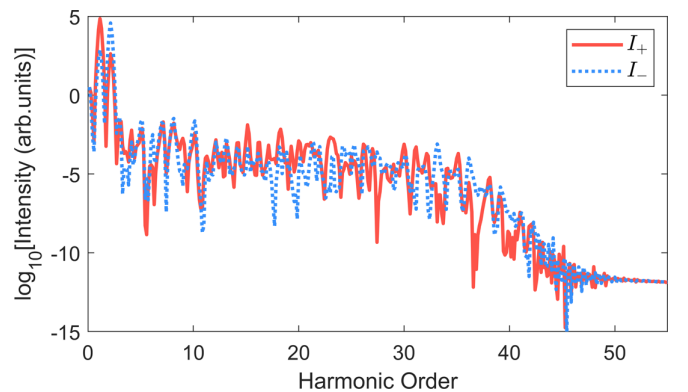


FIG. 5. The spectra of the left-circularly-polarized harmonics (blue dashed line) and the right-circularly-polarized harmonics (red solid line) from CO molecules in the BCCP field.

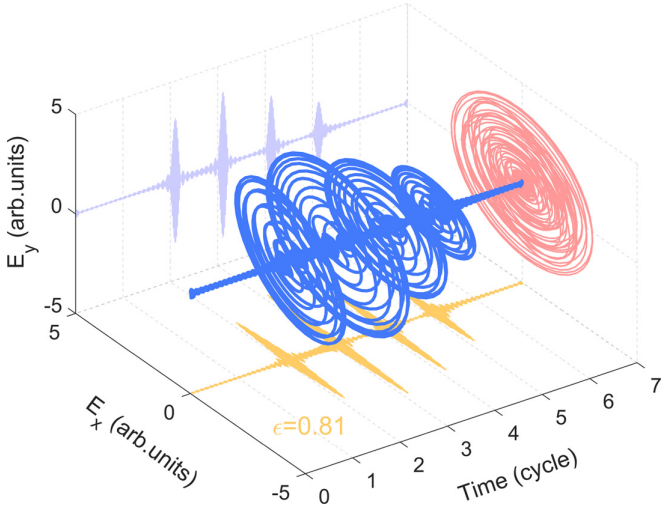


FIG. 6. The 3D plot of the electric field of the APT generated by superposing the 49th-order to the 59th-order harmonics.

projections of the electric field onto the Time- E_x plane and the Time- E_y plane are presented. The projection onto the E_x - E_y plane is also plotted, from which we calculate the ratio of the minor axis to the major axis of the elliptically polarized attosecond fields and the ellipticity ϵ of the APT is around 0.81.

According to Figs. 4(c) and 4(d), harmonic ellipticity for the long trajectory is higher than that for the short trajectory. To further discuss the harmonics for the long and short trajectories, we use the Gabor transform to isolate the contributions from long or short trajectory in the TDSE results [49]. The corresponding harmonic intensity is obtained from the coherent sum over the relevant time windows at times $[t_j, t_j + \Delta t]$ that contribute to the long or short trajectory, respectively. $j = 1, 2, 3, 4$ denotes the four windows in the four optical cycles in the plateau of the trapezoidal pulse

$$I_{GT}(\Omega) = I_{GT_x}(\Omega) + I_{GT_y}(\Omega) = \sum_{q=x,y} \left| \sum_{j=1}^4 \bar{G}T_q[\Omega, t_j] \right|^2 \quad (17)$$

with $\bar{G}T_q(\Omega, t_j) = \int_{t_j}^{t_j + \Delta t} dt GT_q[\Omega, t]$. From this, we obtain the HHG for the long and short trajectories, respectively, as shown in Figs. 7(a) and 7(b). The left- and right-circularly-polarized harmonics are presented by blue dashed and red solid lines. 3D plots of the electric field of the generated APTs are presented in Figs. 7(c) and 7(d). As for harmonics for the long trajectory, the intensity of the right-circularly-polarized component is six orders of magnitude larger than that of the left-circularly-polarized component ranging from the 49th order to the 59th order. One can see the smaller helicity difference in the case of the short trajectory as compared to that for the long trajectory. The calculated ellipticities ϵ of the APTs for the long and short trajectories are around 0.86 and 0.75, respectively. One sees that the ellipticity of the APT for the long trajectory is even higher than that of the generated APT from the total harmonics in Fig. 6. Therefore, if one wants to further improve the ellipticity, a higher harmonic ellipticity can be obtained by filtering the long trajectory. In

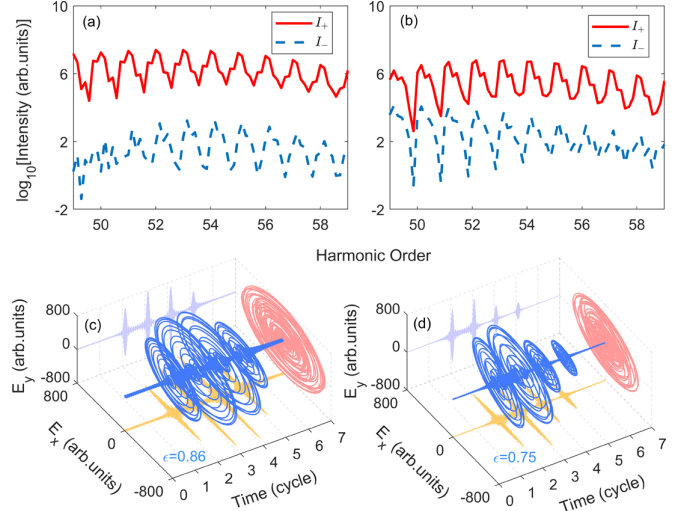


FIG. 7. The HHG and APTs contributing from the long and short trajectories. (a) The HHG contributing from the long trajectory. (b) The HHG contributing from the short trajectory. (c) 3D plot of the electric field of the generated APT contributing from the long trajectory. (d) 3D plot of the electric field of the generated APT contributing from the short trajectory.

the following discussions, we do not filter the short or long trajectory and still consider the total harmonic spectrum.

It is possible to produce highly elliptically polarized IAPs by using shorter LPCP driving field. A sin-squared envelope $\sin^2(\frac{\pi t}{T})$ is used to characterize the pulse profile. We set the width of the driving pulse as $T = 10 T_0$ where the FWHM of the driving pulse is about 9.7 fs. The relative phase $\Delta\phi$ is 0.30π . The HHG of right- and left-circularly polarized components are presented in Fig. 8(a). The intensity of the right-circularly polarized component is much larger than that

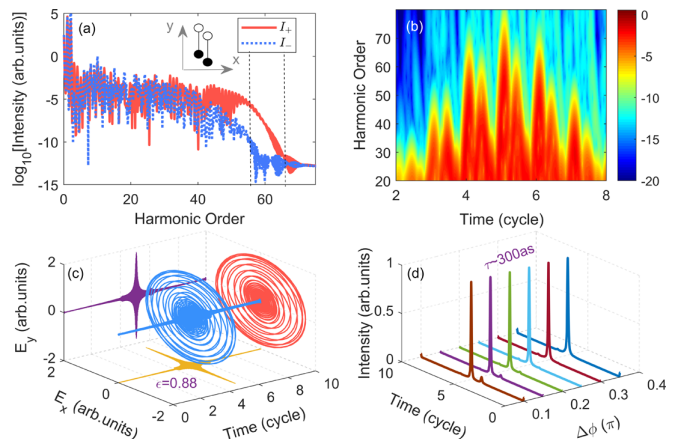


FIG. 8. Results of HHG from CO molecules driven by the shorter LPCP pulse. (a) The spectra of the left-circularly-polarized harmonics (blue dashed line) and the right-circularly-polarized harmonics (red solid line). (b) The time-frequency distribution of the HHG. (c) The 3D plot of the electric field of the IAP generated by superposing the 55th-order to the 65th-order harmonics. (d) The temporal profiles of IAPs in the cases of $\Delta\phi = 0.10\pi, 0.15\pi, 0.20\pi, 0.25\pi, 0.30\pi, 0.35\pi$.

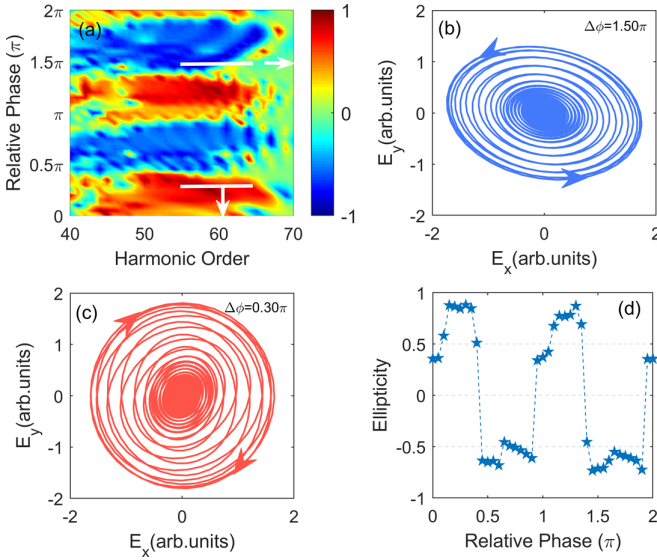


FIG. 9. The ellipticity of high-order harmonics and IAPs versus different $\Delta\phi$. (a) The ellipticity distribution as a function of $\Delta\phi$ and harmonic order. (b), (c) Electric fields of the synthesized IAPs onto the E_x - E_y plane for $\Delta\phi = 1.50\pi$, 0.30π corresponding to the regions marked by the white thick lines in Fig. 9(a). The arrows in the electric field curves label the direction of rotation. (d) The ellipticities of IAPs as a function of $\Delta\phi$.

of the left-circularly polarized component in the range from the 55th-order (presented by the dashed line) to the 65th-order (presented by the dashed line). We present the time-frequency distribution of the harmonic spectra in Fig. 8(b) corresponding to the HHG of Fig. 8(a). The color map of Fig. 8(b) represents the time-frequency distribution in the logarithmic scale. The time-frequency distribution shows that the cutoff energy of one burst around the fifth optical cycle is much higher than those of the other bursts so that there is only one harmonic radiation burst ranging from the 55th order to the 65th order. Therefore, a single pulse can be obtained by filtering the spectra close to the cutoff region. 3D plot of the electric field of the synthesized IAP is presented in Fig. 8(c). The projections of the electric field onto the Time- E_x plane, the Time- E_y plane, and the E_x - E_y plane are also presented. According to the ratio of the minor axis to the major axis of the field, the ellipticity ϵ of the IAP is 0.88. In Fig. 8(d), we show that the temporal profiles of IAPs in the cases of $\Delta\phi = 0.10\pi$, 0.15π , 0.20π , 0.25π , 0.30π , 0.35π . It is shown that the ellipticities of the IAPs are $\epsilon \approx 0.60, 0.86, 0.84, 0.82, 0.88, 0.83$, respectively, and the pulse durations are around 300 as.

By adjusting the relative phase $\Delta\phi$ ranging from 0 to 2π , the ellipticity of the IAPs can be effectively tuned. The ellipticity distribution as a function of $\Delta\phi$ and harmonic order is presented in Fig. 9(a). The red color represents positive ellipticities, which indicates that the high-order harmonics are right-elliptically polarized. The blue color represents negative ellipticities, which indicates that the high-order harmonics are left-elliptically polarized. One can see that the ellipticities are modulated by the relative phase with a period of π . The harmonic ellipticities remain around 0.70 ranging from $\Delta\phi = 0$ to $\Delta\phi = 0.50\pi$ and -0.60 ranging from $\Delta\phi = 1.40\pi$ to

$\Delta\phi = 1.90\pi$. Therefore, the IAPs with the opposite helicities can be produced. The electric fields of two typical IAPs by superposing a series of high-order harmonics (from the 55th order to the 65th order) for $\Delta\phi = 1.50\pi$ and 0.30π are presented in Figs. 9(b) and 9(c). The ellipticities of the two IAPs calculated from the ratio of the minor axis to the major axis of the electric field are -0.73 and 0.88 , respectively. To clearly exhibit the variation of the ellipticities of the IAPs, we present the ellipticities of the obtained IAPs in Fig. 9(d), as a function of $\Delta\phi$ ranging from 0 to 2π . One can see that the ellipticity of the IAP will be tuned rapidly from -0.73 to 0.88 by changing the relative phase.

C. Molecular orientation distribution

Our scheme requires orientation of the molecules, but a practical orientation in experiments cannot be perfect. Therefore, it is necessary to consider the molecular orientation distribution [50–52]. Specifically, the molecular orientation can be achieved by applying a one-color alignment pulse followed by a two-color orientation pulse [50]. We assume that the same molecular orientation distribution is obtained by following the approach introduced in Ref. [50]. The orientation distribution is presented in Fig. 10(a). From this, the time-dependent dipole acceleration $A_q(t)$ is coherently averaged over the molecular axis distribution. We present the HHG considering the orientation distribution in Fig. 10(b). Compared to the results with a fixed orientation, one can see the main feature of the HHG remains the same, while the ellipticity is decreased due to the imperfect orientation. An elliptically polarized IAP can be obtained by filtering the harmonics from the 49th order to the 59th order. The 3D plot of the electric field of the generated IAP is presented in Fig. 10(c) and the ellipticity ϵ of the IAP is 0.56. By further optimizing the orientation, the ellipticity is expected to be further improved.

In addition, we also consider other configurations. Figure 11(a) presents the HHG spectrum when the CO molecules are aligned but not oriented. One can see that the intensity of the right-circularly-polarized component is larger than that of the left-circularly-polarized component ranging from the 49th order (presented by the dashed line) to the 59th order (presented by the dashed line). The IAP obtained by synthesizing this spectral range is shown in Fig. 11(c), with the ellipticity of 0.55. The results indicate that, although the ellipticity is smaller than that for oriented molecules, elliptically polarized IAP can still be obtained close to the cutoff region. Therefore, if a much higher harmonic ellipticity is not demanded, one can choose molecules aligned but not oriented to simplify the experiment. We also study the case when the CO molecules are oriented along the x axis as shown in Figs. 11(b) and 11(d). Elliptically polarized AP can be obtained by filtering the harmonics from the 35th order (presented by the dashed line) to the 45th order (presented by the dashed line) while the ellipticity is dramatically decreased in the range from the 55th order to the 65th order. The result shows that the HHG is sensitive to the molecular orientation and one can adjust the harmonic ellipticity by changing the orientation angle.

Although our scheme requires one more step, i.e., the orientation, in experiment than some methods (for example,

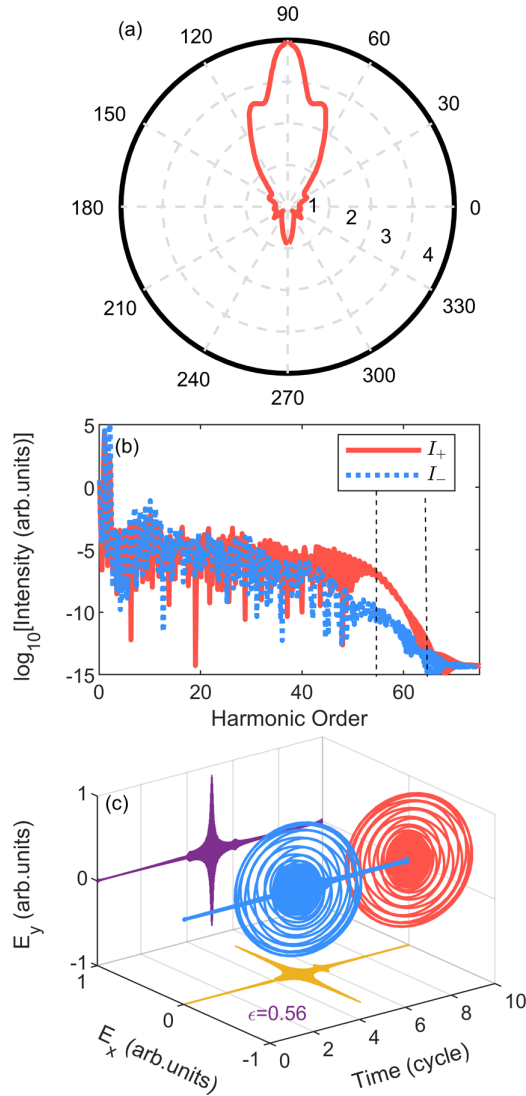


FIG. 10. The HHG and IAP considering the molecular orientation distribution. (a) The molecular orientation distribution. (b) The spectra of the left-circularly-polarized harmonics (blue dashed line) and the right-circularly-polarized harmonics (red solid line) considering the oriented axis distribution. (c) 3D plot of the electric field of the generated IAP.

when atomic noble gas is used as the HHG target), those methods have their own drawbacks, for example, smaller ellipticity of the synthesized AP, as discussed in the Introduction. In our method, the HHG in LPCP field from CO molecules results in a broadband high harmonics spectrum with high average ellipticity. Our method is favorable for applications when one needs the broadband highly elliptically polarized radiation. One should choose a suitable method according to the demand. With the improvement of techniques, it has been easier to achieve the orientation of polar molecules (for example, CO, OCS) nowadays [50–52].

IV. CONCLUSION

In summary, we proposed a method for producing highly elliptically polarized APs from CO molecules using an LPCP

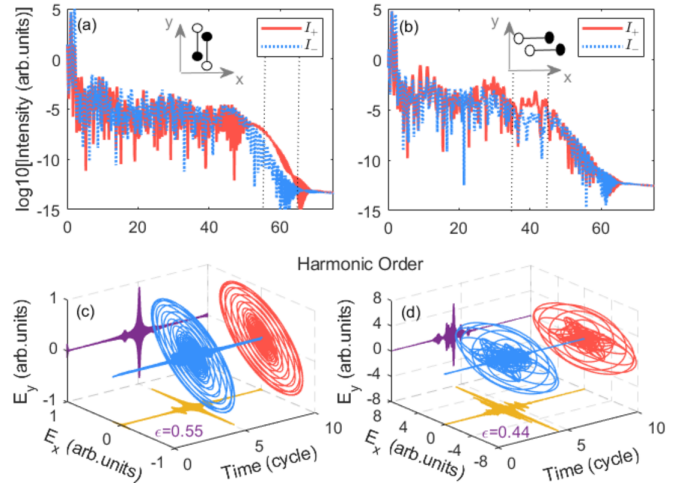


FIG. 11. The HHG and IAPs from CO aligned along the y axis and oriented along the x axis. (a) The spectra of the left-circularly-polarized harmonics (blue dashed line) and the right-circularly-polarized harmonics (red solid line) from CO aligned along the y axis. (b) The spectra of the left-circularly-polarized harmonics (blue dashed line) and the right-circularly-polarized harmonics (red solid line) from CO oriented along the x axis. (c) 3D plot of the electric field of the generated IAP from CO aligned along the y axis. (d) 3D plot of the electric field of the generated AP from CO oriented along the x axis.

driving laser field. By performing a time-frequency analysis of the harmonic spectra and ellipticity, calculating the classical recombination paths and comparing the induced dipole moments from CO and Kr, we find that the phenomenon is due to the manipulation of the classical electron trajectory by the LPCP laser field and the molecular asymmetric structure. We demonstrate that the LPCP laser field leads to an asymmetric recombination so that one of three bursts per cycle has the highest recombination energy than the other bursts. In additions, due to molecular asymmetric orbital, the induced dipole moments D_q^\pm contributing to the right- and left-circularly-polarized harmonics are significantly different. Because of the difference of harmonic ellipticities contributed to by the long and short trajectories, an even higher harmonic ellipticity can be obtained by filtering the long trajectory. Last but not least, by adjusting the relative phase between LP and CP fields, the ellipticities of the IAPs can be tuned in a wide range.

ACKNOWLEDGMENTS

We gratefully acknowledge valuable discussions with Shengjun Yue. This work was supported by National Key Research and Development Program (Grant No. 2017YFE0116600); the National Natural Science Foundation of China (NSFC) (Grants No. 11627809, No. 11874165, No. 91950202, and No. 11774109); Science and Technology Planning Project of Guangdong Province (Grant No. 2018B090944001); the Program for HUST Academic Frontier Youth Team. Numerical simulations presented in this paper were carried out using the High Performance Computing experimental testbed in SCTS/CGCL.

- [1] P. B. Corkum and F. Krausz, *Nat. Phys.* **3**, 381 (2007).
- [2] F. Krausz and M. Ivanov, *Rev. Mod. Phys.* **81**, 163 (2009).
- [3] H. Niikura and P. Corkum, *Attosecond and Angstrom Science, Advances in Atomic, Molecular, and Optical Physics*, edited by P. Berman, C. Lin, and E. Arimondo, Vol. 54 (Academic, New York, 2007), pp. 511–548.
- [4] R. Kienberger, M. Hentschel, M. Uiberacker, C. Spielmann, M. Kitzler, A. Scrinzi, M. Wieland, T. Westerwalbesloh, U. Kleineberg, U. Heinzmann, M. Drescher, and F. Krausz, *Science* **297**, 1144 (2002).
- [5] Y. Pertot, C. Schmidt, M. Matthews, A. Chauvet, M. Huppert, V. Svoboda, A. von Conta, A. Tehlar, D. Baykusheva, J.-P. Wolf, and H. J. Wörner, *Science* **355**, 264 (2017).
- [6] D. Wang, X. Zhu, H. Yuan, P. Lan, and P. Lu, *Phys. Rev. A* **101**, 023406 (2020); S. Luo, M. Li, W. Xie, K. Liu, Y. Feng, B. Du, Y. Zhou, and P. Lu, *ibid.* **99**, 053422 (2019).
- [7] J. Itatani, J. Levesque, D. Zeidler, H. Niikura, H. Pépin, J. C. Kieffer, P. B. Corkum, and D. M. Villeneuve, *Nature* **432**, 867 (2004).
- [8] O. Smirnova, Y. Mairesse, S. Patchkovskii, N. Dudovich, D. Villeneuve, P. Corkum, and M. Y. Ivanov, *Nature* **460**, 972 (2009).
- [9] S. Baker, J. S. Robinson, C. A. Haworth, H. Teng, R. A. Smith, C. C. Chirilă, M. Lein, J. W. G. Tisch, and J. P. Marangos, *Science* **312**, 424 (2006).
- [10] P. M. Kraus, B. Mignolet, D. Baykusheva, A. Rupenyau, L. Horný, E. F. Penka, G. Grassi, O. I. Tolstikhin, J. Schneider, F. Jensen, L. B. Madsen, A. D. Bandrauk, F. Remacle, and H. J. Wörner, *Science* **350**, 790 (2015).
- [11] P. Lan *et al.*, *Phys. Rev. Lett.* **119**, 033201 (2017); B. Wang *et al.*, *Opt. Express* **27**, 30172 (2019).
- [12] S. Ghimire, A. D. DiChiara, E. Sistrunk, P. Agostini, L. F. DiMauro, and D. A. Reis, *Nat. Phys.* **7**, 138 (2011).
- [13] B. Zaks, R. B. Liu, and M. S. Sherwin, *Nature* **483**, 580 (2012).
- [14] L. Li, P. Lan, X. Zhu, T. Huang, Q. Zhang, M. Lein, and P. Lu, *Phys. Rev. Lett.* **122**, 193901 (2019); J. Li, Q. Zhang, L. Li, X. Zhu, T. Huang, P. Lan, and P. Lu, *Phys. Rev. A* **99**, 033421 (2019).
- [15] P. M. Paul, E. S. Toma, P. Breger, G. Mullot, F. Augé, P. Balcou, H. G. Muller, and P. Agostini, *Science* **292**, 1689 (2001).
- [16] M. Hentschel, R. Kienberger, C. Spielmann, G. A. Reider, N. Milosevic, T. Brabec, P. Corkum, U. Heinzmann, M. Drescher, and F. Krausz, *Nature* **414**, 509 (2001).
- [17] G. Sansone, E. Benedetti, F. Calegari, C. Vozzi, L. Avaldi, R. Flammini, L. Poletto, P. Villoresi, C. Altucci, R. Velotta, S. Stagira, S. De Silvestri, and M. Nisoli, *Science* **314**, 443 (2006).
- [18] M. Uiberacker, T. Uphues, M. Schultze, A. J. Verhoef, V. Yakovlev, M. F. Kling, J. Rauschenberger, N. M. Kabachnik, H. Schröder, M. Lezius, K. L. Kompa, H. G. Muller, M. J. J. Vrakking, S. Hendel, U. Kleineberg, U. Heinzmann, M. Drescher, and F. Krausz, *Nature* **446**, 627 (2007).
- [19] A. Ferré, C. Handschin, M. Dumergue, F. Burgy, A. Comby, D. Descamps, B. Fabre, G. A. Garcia, R. Géneaux, L. Merceron, E. Mével, L. Nahon, S. Petit, B. Pons, D. Staedter, S. Weber, T. Ruchon, V. Blanchet, and Y. Mairesse, *Nat. Photon.* **9**, 93 (2015).
- [20] N. Böwering, T. Lischke, B. Schmidtke, N. Müller, T. Khalil, and U. Heinzmann, *Phys. Rev. Lett.* **86**, 1187 (2001).
- [21] D. D. Hickstein, F. J. Dollar, P. Grychtol, J. L. Ellis, R. Knut, C. Hernández-García, D. Zusin, C. Gentry, J. M. Shaw, T. Fan, K. M. Dorney, A. Becker, A. Jaroń-Becker, H. C. Kapteyn, M. M. Murnane, and C. G. Durfee, *Nat. Photon.* **9**, 743 (2015).
- [22] O. Kfir, P. Grychtol, E. Turgut, R. Knut, D. Zusin, D. Popmintchev, T. Popmintchev, H. Nembach, J. M. Shaw, A. Fleischer, H. Kapteyn, M. Murnane, and O. Cohen, *Nat. Photon.* **9**, 99 (2015).
- [23] Y. Li, X. Zhu, Q. Zhang, M. Qin, and P. Lu, *Opt. Express* **21**, 4896 (2013).
- [24] Z. Chang, *Phys. Rev. A* **70**, 043802 (2004).
- [25] X. Xie, A. Scrinzi, M. Wickenhauser, A. Baltuška, I. Barth, and M. Kitzler, *Phys. Rev. Lett.* **101**, 033901 (2008).
- [26] X. Zhang, L. Li, X. Zhu, K. Liu, X. Liu, D. Wang, P. Lan, I. Barth, and P. Lu, *Phys. Rev. A* **98**, 023418 (2018).
- [27] K.-J. Yuan and A. D. Bandrauk, *J. Phys. B* **45**, 074001 (2012); *Phys. Rev. A* **83**, 063422 (2011).
- [28] L. Medišauskas, J. Wragg, H. van der Hart, and M. Y. Ivanov, *Phys. Rev. Lett.* **115**, 153001 (2015).
- [29] D. B. Milošević, *Opt. Lett.* **40**, 2381 (2015).
- [30] K. M. Dorney, J. L. Ellis, C. Hernández-García, D. D. Hickstein, C. A. Mancuso, N. Brooks, T. Fan, G. Fan, D. Zusin, C. Gentry, P. Grychtol, H. C. Kapteyn, and M. M. Murnane, *Phys. Rev. Lett.* **119**, 063201 (2017).
- [31] A. Fleischer, O. Kfir, T. Diskin, P. Sidorenko, and O. Cohen, *Nat. Photon.* **8**, 543 (2014).
- [32] C. Hernández-García, C. G. Durfee, D. D. Hickstein, T. Popmintchev, A. Meier, M. M. Murnane, H. C. Kapteyn, I. J. Sola, A. Jaron-Becker, and A. Becker, *Phys. Rev. A* **93**, 043855 (2016).
- [33] P.-C. Huang, C. Hernández-García, J.-T. Huang, P.-Y. Huang, C.-H. Lu, L. Rego, D. D. Hickstein, J. L. Ellis, A. Jaron-Becker, A. Becker, S.-D. Yang, C. G. Durfee, L. Plaja, H. C. Kapteyn, M. M. Murnane, A. H. Kung, and M.-C. Chen, *Nat. Photon.* **12**, 349 (2018).
- [34] M. Feit, J. Fleck, and A. Steiger, *J. Comput. Phys.* **47**, 412 (1982).
- [35] Y. J. Chen, L. B. Fu, and J. Liu, *Phys. Rev. Lett.* **111**, 073902 (2013).
- [36] J. L. Krause, K. J. Schafer, and K. C. Kulander, *Phys. Rev. A* **45**, 4998 (1992).
- [37] S. Odžak and D. B. Milošević, *Phys. Rev. A* **92**, 053416 (2015).
- [38] X. Zhang, X. Zhu, X. Liu, D. Wang, Q. Zhang, P. Lan, and P. Lu, *Opt. Lett.* **42**, 1027 (2017).
- [39] C. C. Chirilă, I. Dreisigacker, E. V. van der Zwan, and M. Lein, *Phys. Rev. A* **81**, 033412 (2010).
- [40] P. B. Corkum, *Phys. Rev. Lett.* **71**, 1994 (1993).
- [41] I. Barth and M. Lein, *J. Phys. B* **47**, 204016 (2014).
- [42] X. Zhu, P. Lan, K. Liu, Y. Li, X. Liu, Q. Zhang, I. Barth, and P. Lu, *Opt. Express* **24**, 4196 (2016).
- [43] M. J. Frisch *et al.*, GAUSSIAN 09, Revision A.02, Gaussian, Inc. Wallingford CT 20016.
- [44] D. Baykusheva, S. Brennecke, M. Lein, and H. J. Wörner, *Phys. Rev. Lett.* **119**, 203201 (2017).
- [45] P. Balcou, P. Salières, A. L’Huillier, and M. Lewenstein, *Phys. Rev. A* **55**, 3204 (1997).
- [46] M. Lewenstein, P. Balcou, M. Y. Ivanov, A. L’Huillier, and P. B. Corkum, *Phys. Rev. A* **49**, 2117 (1994).

- [47] D. B. Milošević, W. Becker, and R. Kopold, *Phys. Rev. A* **61**, 063403 (2000).
- [48] M. Qin, X. Zhu, K. Liu, Q. Zhang, and P. Lu, *Opt. Express* **20**, 20181 (2012).
- [49] S. Yue, S. Brennecke, H. Du, and M. Lein (to be published).
- [50] P. M. Kraus, D. Baykusheva, and H. J. Wörner, *Phys. Rev. Lett.* **113**, 023001 (2014).
- [51] L. Holmegaard, J. L. Hansen, L. Kalthøj, S. Louise Kragh, H. Stapelfeldt, F. Filsinger, J. Küpper, G. Meijer, D. Dimitrovski, M. Abu-samha, C. P. J. Martiny, and L. Bojer Madsen, *Nat. Phys.* **6**, 428 (2010).
- [52] S. De, I. Znakovskaya, D. Ray, F. Anis, N. G. Johnson, I. A. Bocharova, M. Magrakvelidze, B. D. Esry, C. L. Cocke, I. V. Litvinyuk, and M. F. Kling, *Phys. Rev. Lett.* **103**, 153002 (2009).